Paper

Spectral Matching Imager Using Correlation Image Sensor

Member	Akira Kimachi	(Osaka Electro-Communication University)
Non-member	Toshihide Imaizumi	(The University of Tokyo)
Non-member	Ai Kato	(The University of Tokyo)
Member	Shigeru Ando	(The University of Tokyo)

This paper proposes a spectrally selective imaging system called "spectral matching imager," which consists of the variable wavelength monochrome light source and the correlation image sensor. The variable wavelength monochrome light source illuminates the scene while sweeping its wavelength with time to expand the spectral reflectance/transmittance function of objects along the time axis. At each pixel, the correlation image sensor produces the correlation in the time domain between the expanded spectral function and a reference spectral function. Consequently, pixels that establish a good spectral match have large values in the output image. The spectral matching imager satisfies 1) high spectral resolution, 2) efficient data compression, and 3) tunability to arbitrary optical filter characteristics. Experimental results demonstrate successful detection of objects having detailed narrowband structures, such as glass pieces doped with rare-earth elements.

Keywords: correlation image sensor, spectroscopy, matched filter, colorimetry, watermarking

1. Introduction

Spectral property serves a strong clue in identifying materials of objects. Therefore, the imaging of spectral reflectance/transmittance functions has recently drawn greater attention, driven by the growing need for digital archives or for precise reflection models for realistic computer graphics [1]. One approach describes the spectral function with a finite number of basis functions. This includes studies on separation and estimation of illumination and reflectance spectra by multichannel cameras [2][3], and estimation of reflectance spectra by use of variable spectral illumination [4]. The other approach pursues much higher spectral resolution by use of a spectrograph imager that expands a 1-D slit image to a 2-D spatial-spectral image on its CCD focal plane [5][6]. Unfortunately, the former approach is greatly limited in spectral resolution whereas the latter suffers the problem of data volume and speed. This trade-off is never solved unless the measurement of spectral function pixel-wise is no more an inevitable step of the object recognition.

To develop a spectral imaging system for object detection that operates in real time without losing spectral resolution, we propose the "spectral matching imager" (Fig. 1). It consists of two key components—the variable wavelength monochrome light source and the correlation image sensor. The light source illuminates the scene with a monochrome light sweeping its wavelength over the visible range with time, thus expanding the spectral function of objects along the time axis. The correlation image sensor [7][8], which produces temporal correlation between incident light intensity $f_{ij}(t)$ and a global reference signal $g(t)$ at each pixel

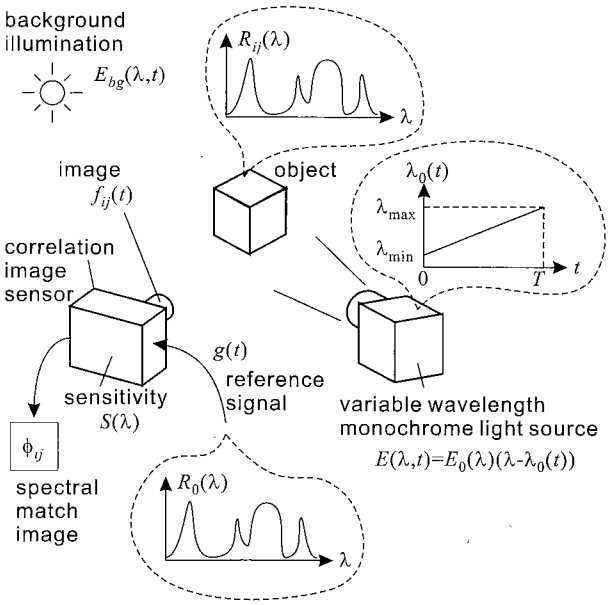

Fig. 1. Schematic illustration of the spectral matching imager.

$$\phi_{ij}(t) = \int_{t-T}^{t} f_{ij}(\tau)g(\tau)d\tau, \quad \cdots\cdots\cdots\cdots\cdots (1)$$

then produces the correlation between the expanded spectral function encoded in $f_{ij}(t)$ and a reference spectral function encoded in $g(t)$ in the time domain. Consequently, pixels that establish a good spectral match have large values in the output image $\phi_{ij}(t)$. From another viewpoint, the spectrum expansion and correlation detection as a whole work as an optical filter characterized by the reference signal $g(t)$. The above sens-

ing architecture allows the spectral matching imager to satisfy the following properties:

- High spectral resolution that is only limited by the peak bandwidth of the monochrome illumination spectrum and the frequency response of the correlation image sensor.
- Efficient data compression through correlation matching in the time domain.
- Tunability to arbitrary optical filter characteristics by choosing the reference signal $g(t)$.

These properties will make the spectral matching imager useful to detection of spectrally watermarked patterns, or discrimination of fake objects based on spectral property.

In the following part of this paper, we first formulate the principle of the spectral matching imager. Next, we describe the design of the imager, with emphasis on the variable wavelength monochrome light source. We then show experimental results and finally summarize this paper.

2. Principle of Spectral Matching Imager

2.1 Spectral Matching on the Corrlation Image Sensor Consider the imaging system in Fig. 1. The variable wavelength monochrome light source illuminates the object with a spectral intensity distribution expressed as a function of wavelength λ and time t:

$$E(\lambda,t)=E_0(\lambda)\delta(\lambda-\lambda_0(t)). \cdots\cdots\cdots\cdots (2)$$

We assume that the peak wavelength $\lambda_0(t)$ sweeps linearly over the range $[\lambda_{\min},\lambda_{\max}]$ during a frame period T of the correlation image sensor:

$$\lambda_0(t)=\frac{\lambda_{\max}-\lambda_{\min}}{T}t+\lambda_{\min}. \cdots\cdots\cdots\cdots (3)$$

The intensity of the incident light at a pixel (i,j) of the correlation image sensor is then given by

$$\begin{aligned} f_{ij}(t) &= \int_0^{\infty}[E(\lambda,t)+E_{bg}(\lambda,t)]R_{ij}(\lambda)S(\lambda)\,d\lambda \\ &= E_0(\lambda_0(t))R_{ij}(\lambda_0(t))S(\lambda_0(t)) \\ &\quad + \int_0^{\infty}E_{bg}(\lambda,t)R_{ij}(\lambda)S(\lambda)d\lambda, \cdots\cdots\cdots (4)\end{aligned}$$

where $R_{ij}(\lambda)$ denotes the spectral diffuse reflectance of the object, $S(\lambda)$ the spectral sensitivity of the correlation image sensor and $E_{bg}(\lambda,t)$ the spectral power distribution of background illumination. We see from the first term of Eq. (4) that the variable wavelength monochrome light has expanded $R_{ij}(\lambda)$ along the time axis.

To take an image on the correlation image sensor, let us create a reference signal $g(t)$ from a reference spectral function $R_0(\lambda)$ as

$$g(t)=\frac{\dfrac{\tilde{R}_0(\lambda_0(t))}{||\tilde{R}_0(\lambda_0(t))||}}{E_0(\lambda_0(t))S(\lambda_0(t))}, \cdots\cdots\cdots\cdots (5)$$

where the tilde $(\sim)$ above $R_0(\lambda)$ denotes its ac component and $||\cdot||$ the ℓ_2 norm and $E_0(\lambda)S(\lambda)\neq 0$ is assumed in $[\lambda_{\min},\lambda_{\max}]$:

$$\tilde{R}_0(\lambda)=R_0(\lambda)-\frac{1}{\lambda_{\max}-\lambda_{\min}}\int_{\lambda_{\min}}^{\lambda_{\max}}R_0(\lambda)d\lambda, \cdots\cdots\cdots\cdots (6)$$

$$||\tilde{R}_0(\lambda)||=\sqrt{\int_{\lambda_{\min}}^{\lambda_{\max}}\tilde{R}_0^2(\lambda)d\lambda}. \cdots\cdots\cdots\cdots (7)$$

With $g(t)$ given by Eq. (5), the background illumination $E_{bg}(\lambda,t)$, which may be daylight, incandescent or fluorescent, is likely to have small temporal correlation with $g(t)$ in general:

$$\int_0^T E_{bg}(\lambda,t)g(t)dt\simeq 0. \cdots\cdots\cdots\cdots (8)$$

Hence, feeding $g(t)$ to the correlation image sensor yields its output as

$$\begin{aligned}\phi_{ij} &\equiv \int_0^T f_{ij}(t)g(t)dt \\ &\simeq \frac{T}{\lambda_{\max}-\lambda_{\min}}\int_{\lambda_{\min}}^{\lambda_{\max}}R_{ij}(\lambda)\frac{\tilde{R}_0(\lambda)}{||\tilde{R}_0(\lambda)||}d\lambda, \cdot (9)\end{aligned}$$

which is just the cross correlation between the spectral functions of the object $R_{ij}(\lambda)$ and reference $\tilde{R}_0(\lambda)/||\tilde{R}_0(\lambda)||$. Note that ϕ_{ij} is independent of the spectral functions of the light source intensity $E_0(\lambda)$ and the sensor sensitivity $S(\lambda)$ thanks to the cancellation by the term $E_0(\lambda_0(t))S(\lambda_0(t))$ in the denominator of $g(t)$. In view of Eqs. (6), (7), the integral in Eq. (9) is rewritten as

$$\begin{aligned}&\int_{\lambda_{\min}}^{\lambda_{\max}}R_{ij}(\lambda)\frac{\tilde{R}_0(\lambda)}{||\tilde{R}_0(\lambda)||}d\lambda \\ &=\int_{\lambda_{\min}}^{\lambda_{\max}}\tilde{R}_{ij}(\lambda)\frac{\tilde{R}_0(\lambda)}{||\tilde{R}_0(\lambda)||}d\lambda \\ &=||\tilde{R}_{ij}(\lambda)||\,\rho(\tilde{R}_{ij}(\lambda),\tilde{R}_0(\lambda)), \cdots\cdots\cdots (10)\end{aligned}$$

where $\rho(\tilde{R}_{ij}(\lambda),\tilde{R}_0(\lambda))$ denotes the correlation coefficient between $\tilde{R}_{ij}(\lambda)$ and $\tilde{R}_0(\lambda)$. Thus, if $||\tilde{R}_{ij}(\lambda)||=1$, ϕ_{ij} yields just the correlation coefficient between $\tilde{R}_{ij}(\lambda)$ and $\tilde{R}_0(\lambda)$, the absolute value of which is maximized when $\tilde{R}_{ij}(\lambda)=k\tilde{R}_0(\lambda)$ (k : constant), that is, the spectral function of the object exactly matches that of the reference except the scale factor. On the other hand, ϕ_{ij} is reduced to zero when $\tilde{R}_{ij}(\lambda)$ is orthogonal to $\tilde{R}_0(\lambda)$.

2.2 Orthogonal Differential Discrimination Suppose that we want to discriminate two objects having different spectral functions $R_1(\lambda)$, $R_2(\lambda)$. We define

$$\tilde{R}_{\pm}(\lambda)=\frac{\tilde{R}_1(\lambda)}{||\tilde{R}_1(\lambda)||}\pm\frac{\tilde{R}_2(\lambda)}{||\tilde{R}_2(\lambda)||}. \cdots\cdots\cdots (11)$$

Note that $\tilde{R}_+(\lambda)$ and $\tilde{R}_-(\lambda)$ are orthogonal (Fig. 2). Then the correlation between $R_1(\lambda)$ or $R_2(\lambda)$ and $\tilde{R}_{\pm}(\lambda)$ yields

$$\int R_1(\lambda)\tilde{R}_{\pm}(\lambda)d\lambda=\frac{1}{2}||\tilde{R}_1(\lambda)||\cdot||\tilde{R}_{\pm}(\lambda)||^2, \cdot (12)$$

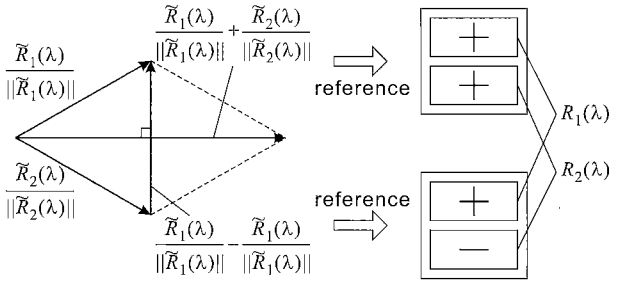

Fig. 2. Vector interpretation of orthogonal differential discrimination of two objects with different spectra.

$$\int R_2(\lambda)\tilde{R}_{\pm}(\lambda)d\lambda = \pm\frac{1}{2}\,||\tilde{R}_2(\lambda)|| \cdot ||\tilde{R}_{\pm}(\lambda)||^2. \quad (13)$$

This means that the reference signal for the differential-mode spectral function $\tilde{R}_{-}(\lambda)$ detects the two objects in opposite polarities, whereas the reference signal for the common-mode spectral function $\tilde{R}_{+}(\lambda)$ detects them in the same polarity. This method helps discriminate an object the spectral function of which has smaller ac energy than that of the other.

2.3 Response to Specular Reflection The derivation in Sec. 2.1 assumed diffuse reflection for surface reflectance $R_{ij}(\lambda)$. It is well known that the surface reflection of inhomogeneous dielectrics such as plastics or opaque glass follows the dichromatic reflection model [1]~[3], which consists of two components—diffuse reflection and specular reflection. In inhomogeneous dielectrics, the spectrum of the specular reflection component coincides with that of the incident light except the scale factor. Taking specular reflection into account, we can modify Eq. (4) as

$$\begin{aligned} f_{ij}(t) &= \int_0^{\infty} [E(\lambda,t) + E_{bg}(\lambda,t)]R_{ij}(\lambda)S(\lambda)\,d\lambda \\ &\quad + r_{ij}\int_0^{\infty} [E(\lambda,t) + E_{bg}(\lambda,t)]S(\lambda)\,d\lambda \\ &= E_0(\lambda_0(t))R_{ij}(\lambda_0(t))S(\lambda_0(t)) \\ &\quad + \int_0^{\infty} E_{bg}(\lambda,t)R_{ij}(\lambda)S(\lambda)d\lambda \\ &\quad + r_{ij}E_0(\lambda_0(t))S(\lambda_0(t)) \\ &\quad + r_{ij}\int_0^{\infty} E_{bg}(\lambda,t)S(\lambda)d\lambda, \cdots\cdots\cdots (14) \end{aligned}$$

where the last two terms account for specular reflection with coefficient r_{ij} denoting its strength. Taking the temporal correlation of these terms with $g(t)$ given by Eq. (5), however, we find that the last term can be eliminated by Eq. (8), and using Eq. (6) we find for the third term

$$\begin{aligned} &\int_0^T E_0(\lambda_0(t))S(\lambda_0(t))g(t)dt \\ &= \int_0^T \frac{\tilde{R}_0(\lambda_0(t))}{||\tilde{R}_0(\lambda_0(t))||}dt \\ &= \frac{T}{\lambda_{\max}-\lambda_{\min}}\int_{\lambda_{\min}}^{\lambda_{\max}} \frac{\tilde{R}_0(\lambda)}{||\tilde{R}_0(\lambda)||}d\lambda = 0. \cdots\cdots (15) \end{aligned}$$

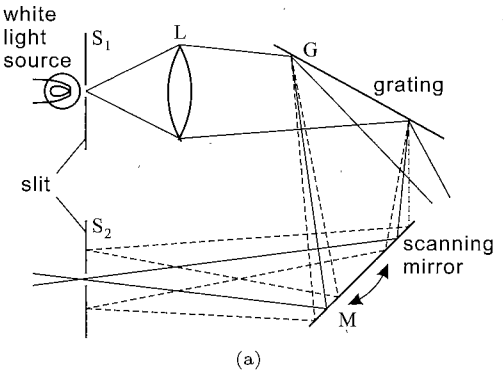

(a)

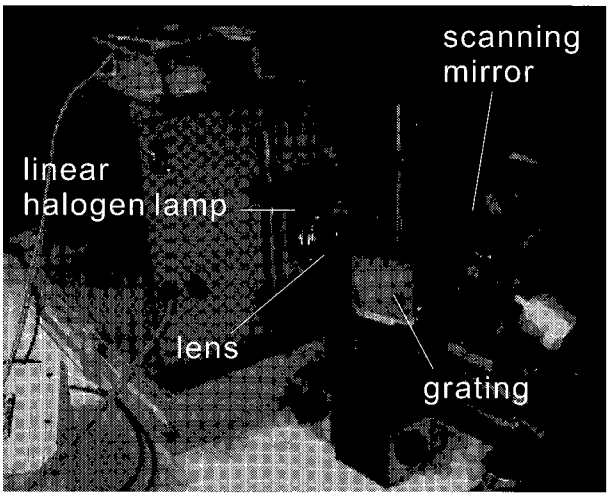

(b)

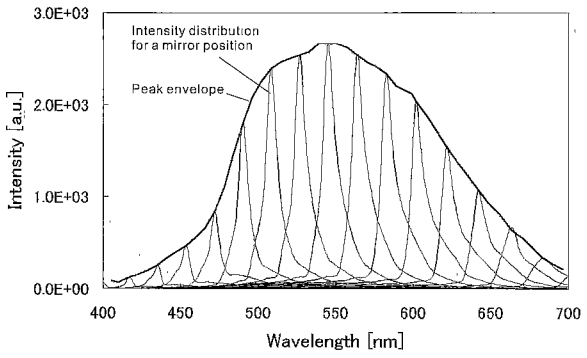

(c)

Fig. 3. Variable wavelength monochrome light source. (a) Optical system using a diffraction grating and a scanning mirror. (b) Photograph of the fabricated light source unit. (c) Measured spectral power distribution of (b) for a number of positions of the scanning mirror, achieving a peak bandwidth of about 15nm. Also plotted is the envelope of the distribution peaks, which corresponds to $E_0(\lambda)$.

Therefore, the spectral matching imager yields only the correlation match with the diffuse reflectance $R_{ij}(\lambda)$ regardless of the presence of specular reflection, as long as the specular reflection component, which usually contains high energy, does not cause nonlinearity in the image sensor outputs by saturation.

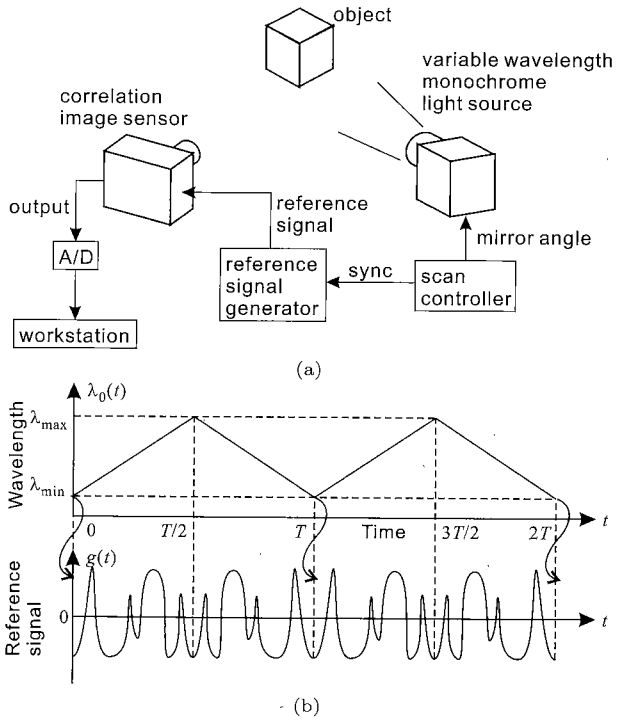

Fig. 4. (a) Expermimental setup of the spectral matching imager. (b) Timing chart of the wavelength of the light source and the reference signal.

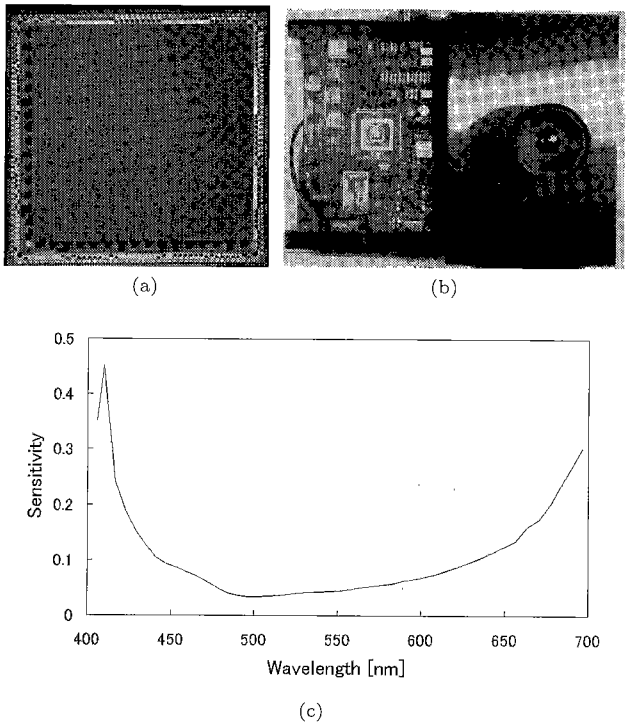

Fig. 5. Correlation image sensor used in this experiment. (a) Photograph of the 64×64-pixel chip. (b) Photograph of the sensor camera. (c) Measured spectral sensitivity $S(\lambda)$ of (a).

3. Variable Wavelength Monochrome Light Source

The simplest design of the variable wavelength monochrome light source would be to diffract a white light and scan the diffracted light directly by moving the grating or prism. Instead, we took an easier implementation as shown in Fig. 3(a), which separately uses a diffraction grating and a scanning mirror that are commercially available.

Based on this design, we fabricated a light source unit as photographed in Fig. 3(b). In order to increase both the intensity and monochromaticity of the diffracted light, we used a 200-W linear halogen lamp as the white light source. Fig. 3(c) plots the measured spectral power distribution of this light source for a number of positions of the scanning mirror, as well as the envelope of the distribution peaks that corresponds to $E_0(\lambda)$. We found that the light source achieves a peak bandwidth of about 15 nm as its spectral resolution, which implies that the spectral matching imager can discriminate spectral functions in a 20-dimensional subspace over the visible range of 400–700 nm. In general, high spectral resolution is desirable for the variable wavelength monochrome light source because the higher the dimension of the subspace of spectral functions, the more precisely spectral matching is performed.

4. Experimental System

Fig. 4(a) shows the experimental setup of the spectral matching imager. The variable wavelength monochrome light source sweeps its wavelength back and forth during each frame period by moving the scanning mirror (General Scanning Inc. XY30M3S + MINISAX Driver). In order to synchronize the reference signal to this scanning scheme, we concatenated the original reference signal and its flipped version along the time axis, and also programmed the scan controller (General Scanning Inc. SC2000) to send the reference signal generator a trigger pulse at the beginning of each scan (Fig. 4(b)).

The correlation image sensor we used in this study has 64×64-pixel resolution (Figs. 5(a)(b)), which was fabricated with a CMOS process provided by VDEC † at the University of Tokyo. The sensor camera in Fig. 5(b) operates under the frame period $T = 1/30$ s. We obtained its spectral sensitivity $S(\lambda)$ in Fig. 5(c) by measurement using the variable wavelength monochrome light source in Fig. 3(b).

5. Experiments

5.1 Discrimination of Color Glass Pieces

We tested the experimental system using color glass pieces doped with rare-earth elements, which are known to introduce detailed narrowband structures into spectral functions. This is why rare-earth elements are often mixed in glaze on ceramic wares to give rise to visual effects such as changes in their apparent color under different illumination spectra. We carried out discrimination tests using metamer glass pieces as well that have much smoother spectral functions despite having almost the same apparent color as that of the rare-earth counterpart.

†VLSI Design and Education Center.
URL: http://www.vdec.u-tokyo.ac.jp/

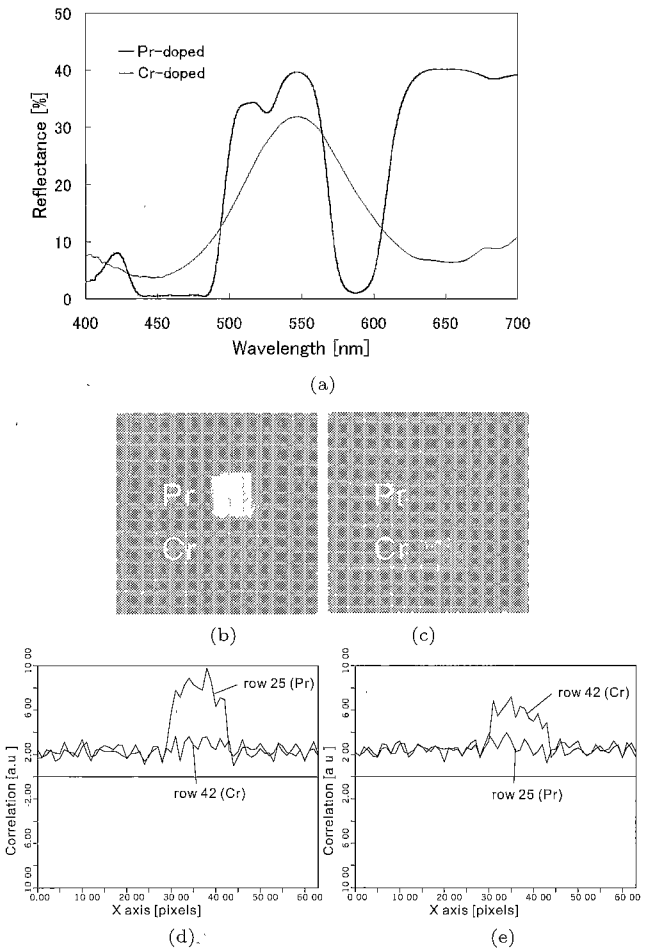

Fig. 6. Results of discrimination of Pr and Cr glasses. (a) Spectral reflectance functions of the glasses. (b)(c) Correlation image outputs for reference signals (b) PR and (c) CR. Top: Pr glass. Bottom: Cr glass. (d)(e) Horizontal cross sections of the correlation image outputs (b) and (c), respectively.

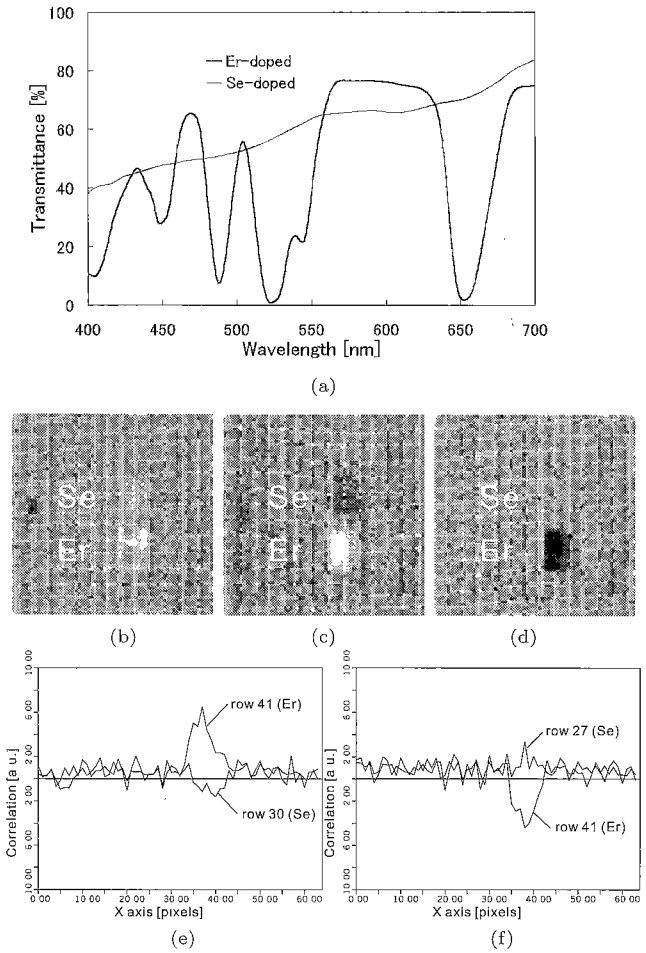

Fig. 7. Results of orthogonal discrimination of Er and Se glasses. (a) Spectral transmittance functions of the glasses. (b)–(d) Correlation image outputs for reference signals (b) ER+SE, (c) ER−SE, and (d) SE−ER. Top: Se glass. Bottom: Er glass. (e)(f) Horizontal cross sections of the correlation image outputs (c) and (d), respectively.

Fig. 6(a) shows the spectral reflectance functions of two glass pieces doped with either Pr (praseodymium), a rare-earth element, or Cr, both of which look green with CIE 1976 $L^*a^*b^*$ color difference [9] $\Delta E^* = 30.3$. The Pr-doped glass piece (let us simply call this "Pr glass") shows much more detailed narrowband structures in its spectral function than the Cr-doped one ("Cr glass"). We generated reference signals from the spectral functions for the Pr glass (let us call this signal PR) and the Cr glass (CR) according to the formula in Eq. (5). Figs. 6(b)(c) show output images of the spectral matching imager captured with reference signals PR and CR, respectively. The upper and lower parts of the images correspond to the Pr and Cr glasses, respectively. Horizontal cross sections of Figs. 6(b)(c) are also plotted in Figs. 6(d)(e). We can observe that only one of the glasses was successfully detected with larger pixel values for its corresponding reference signal as expected.

Next, we examined the orthogonal differential discrimination method proposed in Sec. 2.2, based on transmittance instead of reflectance just described. First, we used two pink glass pieces ($\Delta E^* = 29.8$) doped with either a rare-earth element Er (erbium, "Er glass") or Se ("Se glass"), which have spectral transmitance functions shown in Fig. 7(a). Similarly to Fig. 6(a), the spectral function of the Er glass in Fig. 7(a) has much more detailed narrowband structures. From the waveform in Fig. 7(a) we generated common- and differential-mode reference signals ER+SE, ER−SE following the formula in Eq. (11), with $R_1(\lambda)$ and $R_2(\lambda)$ here denoting the spectral functions of Er and Se, respectively. We then obtained output images for ER+SE, ER−SE and its inverted signal (SE−ER) as shown in Figs. 7(b)–(d). Horizontal cross sections of the differential-mode images in Figs. 7(c)(d) are also plotted in Figs. 7(e)(f). We observe that the regions of the Er (lower part) and Se (upper part) glasses were detected in opposite polarities for the differential-mode reference signals ER−SE and SE−ER, whereas they yielded the same polarity for the common-mode ER+SE. The region for the Se glass has smaller pixel

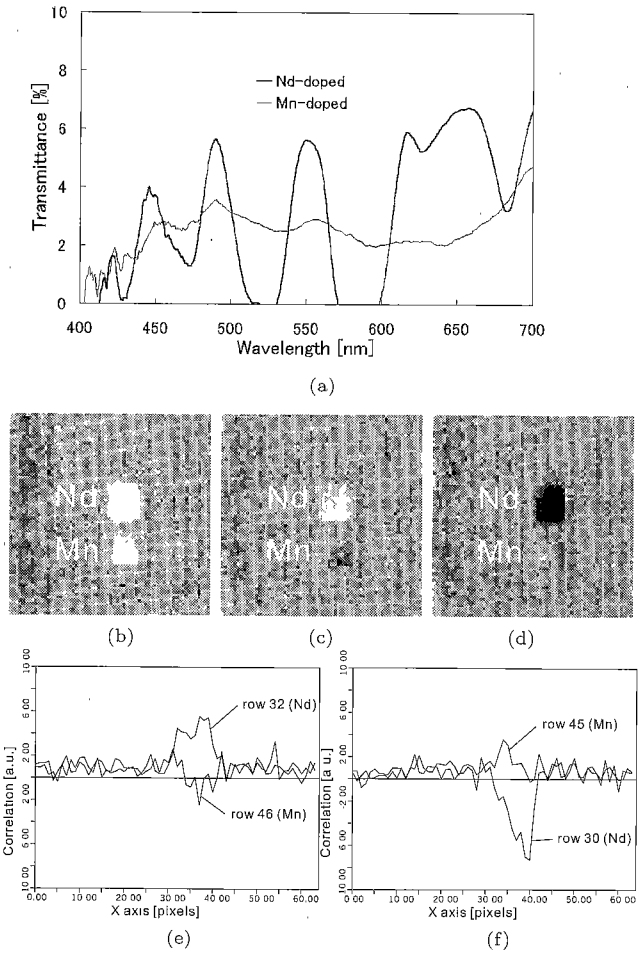

Fig. 8. Results of orthogonal discrimination of Nd and Mn glasses. (a) Spectral transmittance functions of the glasses. (b)–(d) Correlation image outputs for reference signals (b) ND+MN, (c) ND−MN, and (d) MN−ND. Top: Nd glass. Bottom: Mn glass. (e)(f) Horizontal cross sections of the correlation image outputs (c) and (d), respectively.

values than that of the Er glass, which is probably because its spectral function has less energy in its ac component, or $||\tilde{R}_1(\lambda)|| > ||\tilde{R}_2(\lambda)||$, as can be expected from Fig. 7(a).

A similar result was obtained for two purple glass pieces ($\Delta E^* = 26.5$) doped with either a rare-earth element Nd (neodymium, "Nd glass") or Mn-Co ("Mn glass"). For the spectral transmittance functions of the glasses in Fig. 8(a), we obtained the images shown in Figs. 8(b)–(d) (cross sections in Figs. 8(e)(f)) by applying the orthogonal differential discrimination method.

5.2 Application: Detection of Spectral Watermarks We applied the spectral matching imager to detection of spectral watermarks, for which we used a natural green mineral pigment as hidden markers and an artificial one as background. The spectral reflectance functions of these mineral pigments are plotted in Fig. 9(a), showing a significant difference above 650 nm. To detect the regions of the natural mineral pigment, we used a reference signal generated from its

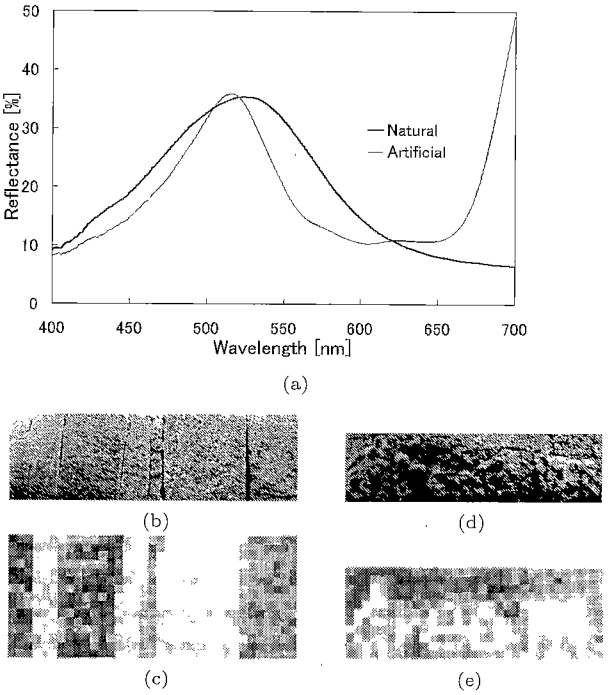

Fig. 9. Detection of watermarks made of natural and artificial green mineral pigments. The output images were taken with a reference signal corresponding to the natural pigment. (a) Spectral reflectance of the green mineral pigments. (b) A hidden barcode-like pattern. (c) Output image for (b) taken with a reference signal for the natural pigment. (d) Hidden characters "d-r-e-a-m." (e) Output image for (d) taken with a reference signal for the natural pigment.

spectral function. Fig. 9(b) shows a photograph of a hidden barcode pattern made of the mineral pigments. For this pattern the spectral matching imager detected only the regions for the natural mineral pigment with positive pixel values, as shown in Fig. 9(c). As another example, Fig. 9(d) shows a photograph of watermarked characters read as "dream." Again, these characters were successfully detected as observed in Fig. 9(e).

6. Summary

We proposed the spectral matching imager, which, consisting of the variable wavelength monochrome light source and the correlation image sensor, performs correlation matching between the spectral functions of an object and a reference at each pixel. It satisfies high spectral resolution, effective data compression and tunability to arbitrary optical filter characteristics. These properties were confirmed in the experiments using color glass pieces doped with rare-earth elements, which have detailed narrowband structures in their spectral functions. We also expect from the experimental results that this imager will be useful to detection of spectrally watermarked patterns as an application.

We thank Sakai Glass Co., Ltd. for providing the glass pieces doped with rare-earth elements.

(Manuscript received June 15, 2001, revised November 30, 2001)

References

(1) S. Tominaga and N. Tanaka, "Estimating reflection parameters from a single color image," *IEEE Computer Graphics and Applications*, vol. **20**, no. 5, pp. 58–66, 2000.

(2) S. Tominaga, "Multichannel vision system for estimating surface and illumination functions," *J. Opt. Soc. Am. A*, vol. **13**, no. 11, pp. 2163–2173, 1996.

(3) S. Tominaga, "Spectral imaging by a multichannel camera," *J. Electronic Imaging*, vol. **8**, no. 4, pp. 332–341, 1999.

(4) M. Hauta-Kasari, K. Miyazawa, S. Toyooka and J. Parkkinen, "Spectral vision system for measuring color images," *J. Opt. Soc. Am. A*, vol. **16**, no. 10, pp. 2352–2362, 1999.

(5) H. M. G. Stokman, Th. Gevers and J. J. Koenderink, "Color measurement by imaging spectrometry," *Comput. Vision Image Understanding*, vol. **79**, pp. 236–150, 2000.

(6) Y. Manabe, S. Kurosaka, O. Oshiro and K. Chihara, "Simultaneous measurement of spectral distribution and shape," *Tech. Digest of 17th Sensor Symp.*, Kawasaki, Japan, May, 2000, pp. 147–150.

(7) S. Ando, T. Nakamura and T. Sakaguchi, "Ultrafast correlation image sensor: concept, design and applications," *IEEE Workshop on CCD and AIS*, Bruges, Belgium, June, 1997.

(8) A. Kimachi and S. Ando, "Time-domain correlation image sensor: first CMOS realization and evaluation," *Proc. Transducers '99*, Sendai, Japan, June, 1999, pp. 958–961.

(9) A. K. Jain, *Fundamentals of Digital Image Processing*. Chap. 3, Prentice-Hall, Englewood Cliffs: NJ, 1989.

Akira Kimachi (Member) received B.E. M.E. and Ph.D. degrees in mathematical engineering and information physics from the University of Tokyo, in 1993, 1995 and 1999, respectively. From 1999 to 2001 he was an assistant professor at the Department of Mathematical Engineering and Information Physics, Graduate School of Engineering, the University of Tokyo. He is currently a lecturer at the Department of Engineering Informatics, Osaka Electro-Communication University. His research interest is in the area of image sensing, image processing and imaging devices. He is a member of IEEJ, SICE and IEICE.

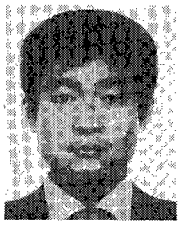

Toshihide Imaizumi (Non-member) received a B.E. degree in mathematical engineering and information physics from the University of Tokyo in 2000. He is currently a graduate student at the Department of Information Physics and Computing, Graduate School of Information Science and Technology, the University of Tokyo. His research interest is in the area of medical sensing and inverse problems.

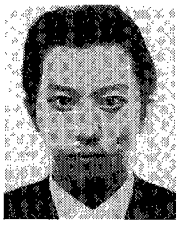

Ai Kato (Non-member) received a B.E. degree in mathematical engineering and information physics from the University of Tokyo in 2000. She is currently a graduate student at the Department of Information Physics and Computing, Graduate School of Information Science and Technology, the University of Tokyo. Her research interest is in the area of medical sensing and inverse problems.

Shigeru Ando (Member) received B.S., M.E. and Ph.D. degrees from the University of Tokyo. From 1987 to 1997, he was an associate professor in mathematical engineering and information physics at the University of Tokyo. He is currently a professor at the Department of Information Physics and Computing, Graduate School of Information Science and Technology, the University of Tokyo. His research and teaching activities have been in the area of smart sensors, vision sensors, auditory sensors, circuits, nonlinear signal processing and image processing. He is a member of IEEJ, SICE, IEEE and OSA.